SPATIAL/SPECTRAL IDENTIFICATION OF ENDMEMBERS FROM AVIRIS DATA USING MATHEMATICAL MORPHOLOGY

Antonio Plaza,[1] Pablo Martínez,[1] J. Anthony Gualtieri,[2] and Rosa M. Pérez[1]

1. INTRODUCTION

During the last several years, a number of airborne and satellite hyperspectral sensors have been developed or improved for remote sensing applications (Green, 1988-2000; Vane et al., 1993; Kruse & Boardman, 1999). Imaging spectrometry allows the detection of materials, objects and regions in a particular scene with a high degree of accuracy. Hyperspectral data typically consist of hundreds of thousands of spectra, so the analysis of this information is a key issue (Landgrebe, 1997).

A very useful and commonly accepted approach to analyze hyperspectral data has been the identification of the purest spectra, or "endmembers" (Kruse, 1998). Some researchers have taken the approach of constructing spectral libraries of pure elements that can be matched with every spectrum in a hyperspectral image in order to classify the scene (Roberts et al., 1999). This processing is suitable when pure materials, contained in the library, are on the ground, but in real-world situations, since materials are spatially or intimately mixed, only the strongest features are matched. As a result, the most widely used technique is to determine endmember spectra directly from the image. Once the individual endmembers have been identified, several methods can be used to map their spatial distributions, associations and abundances (Boardman & Kruse, 1994; Kruse et al., 1996).

A large variety of methodologies have been proposed in the literature in order to find endmembers in the data cube (Winter & Winter, 1999). One of the most successful approaches is the Pixel Purity Index™ (PPI) algorithm (Boardman et al., 1995), which finds the "purest" pixels in the scene through a series of repeated projections on to randomly oriented lines in N-dimensional space. These potential endmember spectra are loaded into an N-dimensional scatterplot and rotated in real time until a trained analyst selects extremities in the data cloud that likely correspond with scene endmembers. This procedure, based on the geometry of convex sets, is widely accepted (available in the commercial software system ENVI®, the Environment for Visualizing Images), but it is time-consuming and highly interactive.

Several methods for autonomous extraction of endmembers have been recently proposed in the literature. The N-FINDR algorithm (Winter & Winter, 1999) finds the simplex of maximum volume that can be enclosed within all the points of the data cloud. The ORASIS algorithm (Palmadesso et al., 1999) uses a process called Exemplar Selection to thin the data set by rejecting any "redundant" spectra (this requires the calculation of the angle between spectral vectors). The Iterative Error Analysis (IEA) approach (Szeredi et al., 1999) performs a series of constrained unmixings and chooses as endmembers those pixels that minimize the error in the unmixed image. In addition to these physically based methods, there are several statistically based approaches that rely on clustering algorithms (Beaven et al., 1999). The major drawback of all the previously addressed methods is that they only consider the spectral information contained in the data cube. Spatial information has not been fully exploited yet, specially in unsupervised classification. The integration of both spatial and spectral information is becoming more relevant as the sensors used in spaceborne platforms tend to increase the spatial resolution (Jiménez & Rivera-Medina, 1999).

Mathematical morphology theory (Serra, 1982) is a widely used non linear technique for image analysis and pattern recognition. Although it is especially well suited to segment binary or grayscale images with irregular and complex shapes, its application in the classification/segmentation of multispectral or hyperspectral images has been quite rare (Soille, 1996; Lambert & Channusot, 2000). In this paper, we discuss a new completely automated methodology to find endmembers in the hyperspectral data cube using mathematical morphology.

[1] Departamento de Informática, Universidad de Extremadura, Avda. de la Universidad s/n, 10071 Cáceres, SPAIN
E-mail: {aplaza, pablomar, rosapere}@unex.es

[2] Global Science and Technology at Applied Information Sciences Branch, NASA/GSFC, Greenbelt, Maryland 20771, U.S.A.
E-mail: gualt@peep.gsfc.nasa.gov

The extension of classic morphology to the hyperspectral domain allows us to integrate spectral and spatial information in the analysis process. In Section 3, some basic concepts about mathematical morphology and the technical details of our algorithm are provided. In Section 4, the accuracy of the proposed method is tested by its application to real hyperspectral data obtained from the AVIRIS imaging spectrometer. Some details about these data and reference results, obtained by well-known endmember extraction techniques, are provided in Section 2. Finally, in Section 5 we expose the main conclusions at which we have arrived.

2. DATA

We have applied our endmember extraction algorithm to real hyperspectral data obtained from the AVIRIS imaging spectrometer for a particular scene: Salinas 98 taken in the Salinas Valley, California on October 9, 1998 (Gualtieri et al., 1999). This data was available only as at-sensor radiance data and includes vegetables, bare soils and vineyard fields. We have selected a subscene of the Salinas 98 dataset called Salinas A, which comprises 83x86 pixels and includes six classes. Ground truth is available for this image (see Figure 5 at the end of the paper).

The spatial characteristics of the Salinas A dataset make it particularly suitable for testing the accuracy of our method. Ground truth information reveals zones where broccoli with weeds, senesced corn and romaine lettuce are present. The romaine lettuce is at different weeks since planting and with growth increasingly covering the soil.

A reference dataset of endmembers was obtained for this particular image using the Pixel Purity Index™ (PPI) procedure as implemented in the commercial software system ENVI®. The endmembers extracted by this widely accepted supervised methodology will be compared to those found by our algorithm. The full ENVI process is detailed next.

First, the spectral data volume of the hyperspectral dataset was reduced by using the Minimum Noise Fraction (MNF) transformation. The top MNF bands, which contain most of the spectral information, were used to determine the most likely endmembers by using the PPI procedure. These potential endmember spectra were loaded into an N-dimensional scatterplot and rotated in real time through the N-Dimensional Visualizer™ until extremities on the scatterplot were found. The resulting projections were annotated and exported to the image using Region-of-Interest (ROI) definition procedures. Mean spectra were extracted for each ROI to act as endmembers for mapping through Linear Spectral Unmixing, which results in a series of grayscale abundance maps (rescaled to lie in the range from 0 to 255), representing the fractional composition of endmember materials in the scene (darker pixels indicate more concentration of the endmember material). The results of applying this methodology to the Salinas A dataset are depicted in Figure 7, where 7.a shows the resulting endmembers and 7.b to 7.e show their correspondent abundance maps.

3. METHODS

In this section we provide some basic concepts about mathematical morphology theory and describe a schema to extend morphological operators to the hyperspectral domain. Finally, we propose an automated methodology, based on morphology, to extract endmembers from the data cube.

3.1 Classic Mathematical Morphology

Mathematical morphology theory (Serra, 1982) has now become an useful tool for image analysis and pattern recognition. In binary morphology, images are represented as sets, where pixels in the image foreground are members of a set X and pixels in the background belong to the complementary set X^C. The two basic operations of mathematical morphology consist of the transformation of an image by another set K, known as the structuring element. The shape and size of the structuring element determine the spatial characteristics of the resulting image. The two basic morphology operations, dilation and erosion, are defined respectively as follows:

$$X \oplus K = \{s \mid K_s \cap X \neq \varnothing\} \tag{1}$$

$$X \otimes K = \{s \mid K_s \subseteq X\} \tag{2}$$

Erosion and dilation are said to be dual to each other with respect to complementation. We call the *opening* of X with respect to K the following set:

$$X_K = (X \otimes K) \oplus K \tag{3}$$

Similarly, we call the *closing* of X with respect to K the following set:

$$X^K = (X \oplus K) \otimes K \tag{4}$$

The opening of X by K is thus defined in terms of an erosion followed by a dilation. Similarly, the closing of X by K is defined in terms of a dilation followed by an erosion.

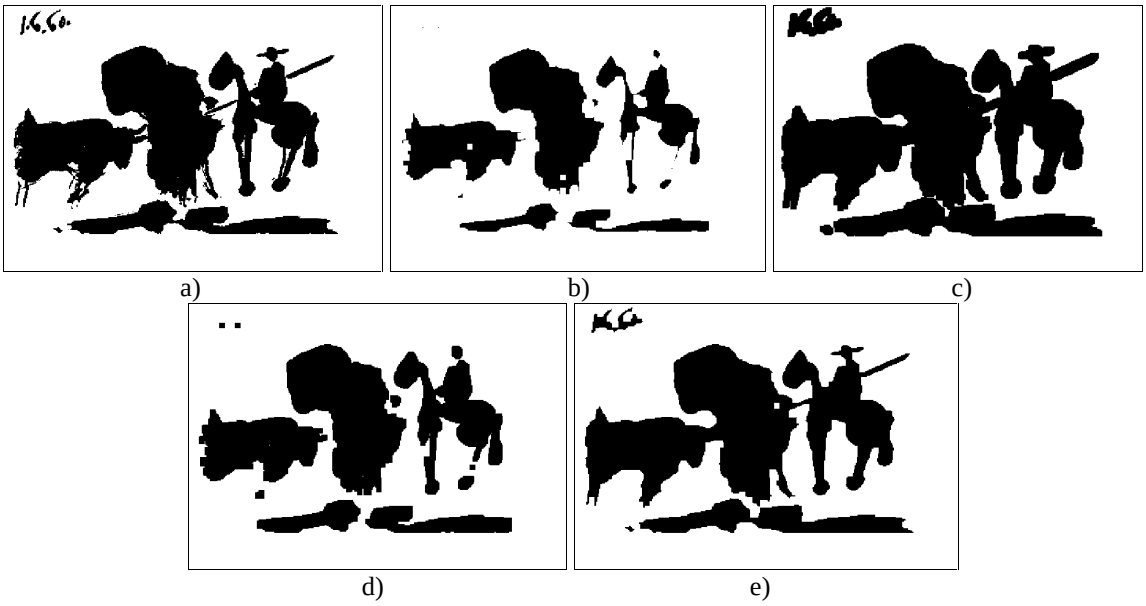

Figure 1. Binary mathematical morphology example.

Figure 1 shows the effect of applying erosion and dilation operations to a simple binary image corresponding to an original Pablo Picasso painting: "Pass with the cape," 1960 (Figure 1.a). In 1.b and 1.c, the results of applying a binary erosion and a binary dilation to 1.a with a 5x5 square-shaped structuring element are respectively addressed. Finally, in 1.d and 1.e the effect of opening and closing image 1.a with the same structuring element are shown. As depicted in Figure 1, after having eroded X by K, it is not possible, in general, to recover the initial set by dilating the eroded set by the same K, i.e. $(X \otimes K) \oplus K$. This dilate reconstitutes only a part of X which is simpler and has less details, but the new set, called the *opening* of X, actually filters out a subset of X which is extremely rich in morphological and size distribution properties (Serra, 1993).

The principles of mathematical morphology have also been extended to the grayscale image case (Sternberg, 1986). Greyscale images are described as a grey level function $f(x, y)$ on the points of Euclidean 2-space. Grayscale dilation, erosion, opening and closing are respectively defined as follows:

$$(f \oplus k)(x, y) = \underset{(s,t)\in k}{\text{Max}} \{f(x - s, y - t) + k(s, t)\} \quad (5)$$

$$(f \otimes k)(x, y) = \underset{(s,t)\in k}{\text{Min}} \{f(x + s, y + t) - k(s, t)\} \quad (6)$$

$$f_k(x, y) = ((f \otimes k) \oplus k)(x, y) \quad (7)$$

$$f^k(x, y) = ((f \oplus k) \otimes k)(x, y) \quad (8)$$

The expressions for greyscale dilation and erosion bear a marked similarity to the convolution integral encountered frequently in digital image processing, with sums and differences replacing multiplication and minimum and maximum replacing summation. Figure 2 illustrates the effect of applying greyscale erosion (2.b), dilation (2.c), opening (2.d) and closing (2.e) to a simple greyscale image (2.a), using a 5x5 square-shaped structuring element. As it can be infered from this example, image processing through iterative morphological transformation is a process of selective information removal where irrelevant image content is irrecoverably destroyed, enhancing the contrast of image features of certain spatial characteristics (in this sense, the structuring element acts as a *matching pattern* that performs a filtering operation).

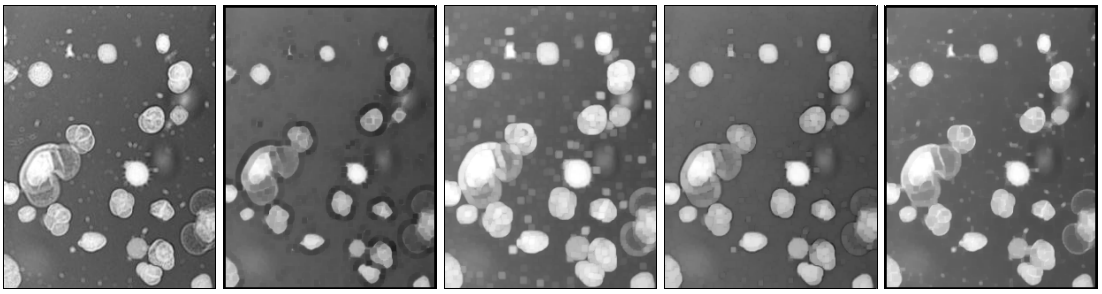

a) b) c) d) e)

Figure 2. Greyscale mathematical morphology example.

3.2 Extending mathematical morphology to N-dimensional space

Mathematical morphology definition requires an algebraic structure T (complex lattice) such that:

a) T is induced by a (partial) ordering relation, and

b) For any family of elements in T, there exists a smallest majorant or *supremum* and a greatest minorant called the *infimum* (Lambert & Chanussot, 2000).

In the case of hyperspectral images, these two properties are missing because there is no natural means for total ordering of multivariate pixels. Two main strategies have been considered in order to solve this:

a) The first one consists of processing each channel of the hyperspectral image separately. This *marginal* approach is not satisfying because it does not take into account the existing correlation between the individual channels.

b) The second one uses a purely vector approach to process the hyperspectral channels all at once. This strategy requires the definition of a vector ordering relation to determine the *supremum* and the *infimum* of any family of N-dimensional vectors.

The definition of a vector ordering relation can be done as follows. Let x_1, x_2, …, x_n be the hyperspectral image pixels within a filtering window that represents the structuring element of a morphological operation. We can define a measure of the dissimilarity between two of those pixels, x_a and x_b by:

$$\mathrm{dist}(x_a, x_b) = \cos^{-1}\left(\frac{x_a \cdot x_b}{\|x_a\| \cdot \|x_b\|}\right) \tag{9}$$

This is the angular distance function, expressed in radians. The following scalar quantity can be calculated to measure the global distance between a particular pixel x_i and a set $x_j, j = 1...m$ of neighboring pixels.

$$d_i = \sum_{j=1}^{m} \mathrm{dist}(x_i, x_j) \tag{10}$$

The *supremum* and *infimum* of a set of $x_i, i = 1...n$ hyperspectral pixels are respectively defined:

$$\sup(x_i) = h = \arg\max_i d_i \tag{11}$$

$$\inf(x_i) = l = \arg\min_i d_i \tag{12}$$

Now it is easy to determine basic morphology operations such as erosion and dilation by *maximum* and *minimum* operations, as described in the previous subsection. While *h* is the most spectrally singular pixel in a spatial neighborhood, *l* is nothing else than the median of the pixels the neighborhood, according to the classical vector median definition (Lambert & Chanussot, 2000).

3.3 Autonomous morphological endmember extraction (AMEE)

We propose a morphology-based automated algorithm to extract endmembers from hyperspectral images. The input to this process is the full hyperspectral image cube, with no previous dimensionality reduction or pre-processing. The procedure must examine the full dataset to find those pure pixels that can be used to describe the various mixed pixels in the scene. This is done in the following steps.

3.3.1 Application of morphological operators

Let X be the original image and K a structuring element. We propose the following morphological operator to identify endmembers:

$$X\Phi K = \mathrm{dist}(X, X^K) = \mathrm{dist}(X, (X \oplus K) \otimes K) \tag{13}$$

This operator works as follows: firstly, a hyperspectral closing operation is applied to the original image; then, a measure of the dissimilarity between each pixel of the original image and the correspondent pixel in the closed image is calculated by the angular distance function.

It is important to emphasize that Φ extracts spectral information using a pixel by pixel basis, much like other existing methods, but the process is guided by spatial information. As a result, the spatial and spectral response is considered simultaneously in the analysis process.

Let K be a square-shaped, 3x3 structuring element. Figure 3 illustrates the working procedure of the operator when applied to a target pixel E in the original image using K as structuring element. Firstly, the most spectrally pure hyperspectral pixel (Q) in a spatial neighborhood of the target pixel is selected after projecting each pixel against all its spatial neighbors. This procedure is repeated for every pixel in X, leading to a new image $X \oplus K$. From this image, only the pixels that provide a good representation of their neighbors are selected by the minimum operator, which in our case is equivalent to a vector median filtering. The pixels in $(X \oplus K) \otimes K$ match the definition of an endmember, i.e. a spectrally pure pixel that can be used to describe several mixed pixels in the scene. Finally, the dissimilarity between E, the target pixel in the original image, and V, the pixel selected by the operator, is calculated to check if the target pixel is likely to be an endmember.

The previously described operation is repeated using structuring elements of progressively increased size, in order to obtain a detailed information of the spatial context associated to each hyperspectral pixel. The overall result of applying a sequence of morphological operators to the original image is a spatial/spectral signature associated to each pixel of the scene. From this information, a 2-dimensional grayscale rule image is generated following the basic idea of the Pixel Purity Index algorithm: those pixels that have been repeatedly selected by the operator during the process increase their probability of being declared "pure".

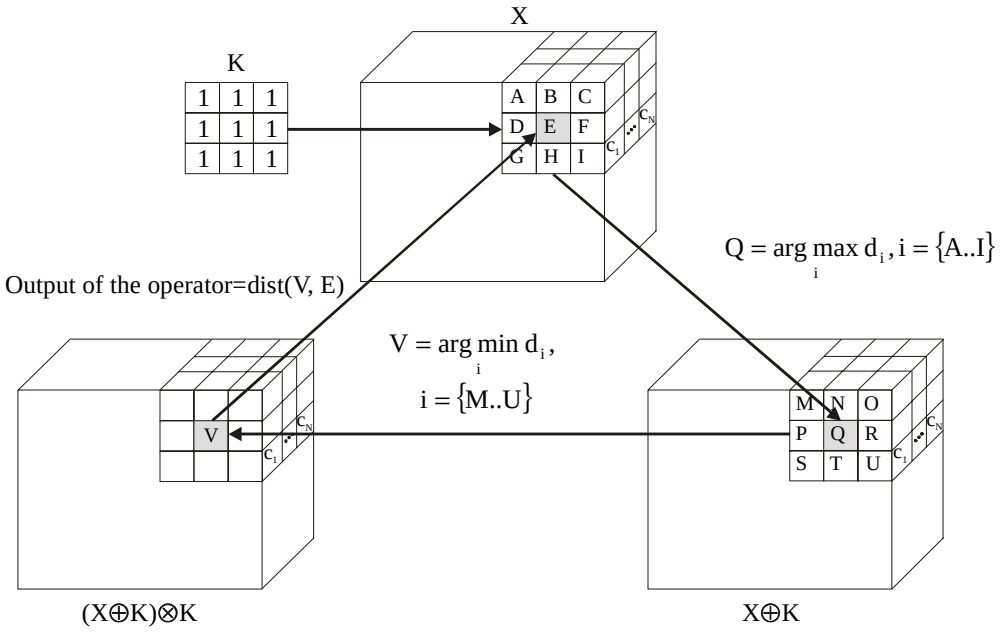

Figure 3. Working procedure of Φ hyperspectral morphological operator.

3.3.2 Endmember selection

Individual endmember spectra can be selected by automatically thresholding the previously obtained rule image. Once the automatical thresholding has been performed, mean spectra can be extracted from the resulting regions to act as endmembers for spectral mapping.

Several methods for automatic thresholding of grayscale images are available in the literature (Sahoo et al., 1988). In our particular case, we have found satisfactory results using Otsu method (Otsu, 1979), which is based on the minimization of the weighted sum of group variances. Let σ_w^2, σ_b^2 and σ_t^2 be the within-class, between-class and total variance, respectively. An optimal threshold v can be determined by maximizing one of the following criterion functions with respect to v:

$$\lambda = \frac{\sigma_b^2}{\sigma_w^2} \qquad \eta = \frac{\sigma_b^2}{\sigma_t^2} \qquad \kappa = \frac{\sigma_t^2}{\sigma_w^2} \tag{14}$$

3.3.3 Redundant endmember thinning

Thresholding of the rule image may result in several unconnected regions with very similar mean spectra, so a procedure to reject redundant endmembers must be performed. We propose to apply a spatial/spectral seeded region growing from those regions, following the approach of Bateson et al., 1998 to create endmember bundles.

The process is as follows: neighboring pixels are incorporated to each region if their spectra are sufficiently correlated to the mean spectrum of the region (a threshold angular distance value A=0.001 is previously set). Once the region growing process has finished, mean spectra associated to the resulting regions are stored in a dataset. If several regions merge during the process, redundant endmember spectra are automatically thinned from the original dataset.

The previously described algorithm performs a spatial/spectral processing of the original image. Spectral information at each pixel is analyzed regarding its spatial context, which guides the fully automated endmember extraction process.

4. RESULTS AND DISCUSSION

In this section, the application of the Autonomous Morphological Endmember Extraction (AMEE) algorithm to hyperspectral data collected by the AVIRIS sensor is discussed. In particular, the Salinas A dataset (see Figure 1) is analyzed. The results obtained by our method are compared to those found using the Pixel Purity Index (PPI) algorithm implemented in the software system ENVI (a detailed explanation of this ENVI-based analysis process can be found in Section 2).

The full AMEE process for this particular image was accomplished in approximately 50 seconds using a Pentium III 500 MHz personal computer with 128 Megabytes of RAM. A sequence of morphological Φ operators with square-shaped structuring elements of size ranging from N_1xN_1 to N_2xN_2 (N_1=3 and N_2=30) was applied to the image in order to create a rule image. Seed regions were extracted by automatically thresholding the rule image and a preliminary set of endmembers was generated. Redundant endmembers were thinned using a seeded region growing process with angular distance parameter A=0.001 (refer to subsection 3.3 for a detailed description of each step).

Figure 4 shows some intermediate results of the processing. The resulting endmembers of applying our methodology to the Salinas A dataset are shown in Figure 6.a, along with grayscale abundance maps (6.b to 6.e) representing the fractional composition of endmember materials in the scene. These maps have been obtained by the Linear Spectral Unmixing procedure using the extracted endmembers, and have been rescaled to lie in the range from 0 to 255. Our results can be visually compared with those found using PPI (Figure 7).

a) b) c)

Figure 4. Intermediate results of processing the Salinas A image with AMEE method. a) Probability image after applying morphological operators to the full hyperspectral dataset. b) Resulting image after automatically thresholding *a* with Otsu method. c) Resulting image after spatial/spectral growing of the seeds obtained in *b*.

For the purpose of comparison, Table 1 shows the correlation matrix between the endmembers obtained by AMEE and PPI methods. This table reveals very high correlation values for endmembers 1, 2 and 3, and a reasonably high correlation value for endmember 4. The availability of ground truth allows us to identify the zones that those endmembers represent: in particular, endmembers 1, 2 and 3 correspond to broccoli, romaine lettuce at 4 weeks and romaine lettuce at 7 weeks. Endmember 4 corresponds to the corn senesced and green weeds zone (there is some variability for this endmember as it can be appreciated in Table 2).

Table 1. Correlation matrix between the endmembers obtained by AMEE and PPI (ENVI-based) methods.

		AMEE endmembers			
		1	2	3	4
PPI Endmembers	1	**0.999**	0.973	0.72	0.735
	2	0.980	**0.999**	0.839	0.852
	3	0.718	0.85	**0.999**	0.998
	4	0.902	0.917	0.938	**0.966**

In order to analyze if the abundance maps shown in Figure 6 are meaningful, we have taken into account the following simple reasoning. Let $P(i, j, \lambda)$ be the radiance at pixel x_{ij} of the original image and wavelength λ. Also, let $p_k(\lambda), k = 1..n$ be the extracted endmember spectra and $a_k(i, j), k = 1..n$ the fractional endmember amounts at hyperspectral pixel x_{ij}. If the selected *n* endmembers are correct, all hyperspectral pixels in the original image can be expressed as a linear combination of fractional endmember amounts, i.e.:

$$\forall i, j, \sum_k a_k(i, j) \cdot p_k(\lambda) = P(i, j, \lambda) \tag{15}$$

The following experiment analyzes the "quality" of the endmembers extracted by both PPI and AMEE methods. According to our previous reasoning, if the endmembers are properly constructed, they represent approximations to the signature patterns of the actual constituents of the scene being observed, i.e. a linear combination of fractional endmember abundances at each pixel of the image must account for all of the original hyperspectral cube radiance. Then, a reconstruction of the original hyperspectral image (or "test" image) can be generated by the dataset of extracted endmembers and their resulting abundance maps, using equation 15. A set of endmembers would be "good" if we can obtain a test image that is very similar to the original. In fact, this remark provides us with a powerful mechanism to compress the full hyperspectral dataset.

Table 2 shows the results of measuring the mean quadratic error (sum of the quadratic error at each pixel divided by the number of pixels) between the original hyperspectral dataset and "test" images generated by PPI and AMEE endmember sets.

Table 2. Mean quadratic error between test images, generated using both PPI and AMEE endmember sets, and the original Salinas A dataset.

	PPI Test Image	*AMEE Test Image*
Original Image	5.66	5.71

The results shown in Table 1 and Table 2 indicate that the proposed methodology is able to obtain very similar results to those found using the supervised procedure implemented in ENVI, but without the necessity of human supervision. This fact leads to an important reduction in the overall analysis time. Although the results obtained for the Salinas A dataset are encouraging, some work is still needed in order to extrapolate our conclusions to other hyperspectral datasets.

5. CONCLUSIONS

We have presented a new autonomous method to find endmembers in hyperspectral remote sensing data based on mathematical morphology concepts. Although no previous dimensionality reduction or data thinning is performed, it is capable of accurate and rapid determination of endmember spectra from high dimensional hyperspectral images. Some preliminary results obtained after applying this algorithm to AVIRIS sensor data show that it is successful in the task of integrating spatial and spectral information in the analysis process.

REFERENCES

Bateson, C.A., Asner, G.P., Wessman, C.A., "Incorporating Endmember Variability into Spectral Mixture Analysis through Endmember Bundles," *Summaries of the Seventh JPL Airborne Earth Science Workshop*, 1998.

Beaven, S., Hoff, L.E., Winter, E.M., "Comparison of SEM and Linear Unmixing Approaches for Classification of Spectral Data", *Proc. SPIE*, 1999.

Boardman, J.W. & Kruse, F.A., "Automated Spectral Analysis: A Geological Example Using AVIRIS Data, Northern Grapevine Mountains, Nevada," *Proc. 10th Thematic Conference, Geologic Remote Sensing*, San Antonio, TX, May 1994.

Boardman, J.W., Kruse, F.A. & Green, R.O., "Mapping Target Signatures via Partial Unmixing of AVIRIS Data," *Summaries of the Fifth JPL Airborne Earth Science Workshop*, 1995.

Green, R.O., Editor, AVIRIS Earth Science Workshop Proceedings, 1988-2000. Available at http://makalu.jpl.nasa.gov/

Gualtieri, J.A., Chettri, R., Cromp, R.F., Johnson, L.F., "Support Vector Machine Classifiers as Applied to AVIRIS Data," *Summaries of the Eighth JPL Airborne Earth Science Workshop*, 1999.

Jiménez, L.O. & Rivera-Medina, J., "On the Integration of Spatial and Spectral Information in Unsupervised Classification for Multispectral and Hyperspectral Data," *Part of the EUROPTO Conference on Sensors, Systems and Next-Generation Satellites, Proc. SPIE*, Florence, Italy, Sep. 1999.

Kruse, F.A. & Boardman, J.W., "Fifteen Years of Hyperspectral Data: Northern Grapevine Mountains, Nevada," *Summaries of the Eighth JPL Airborne Earth Science Workshop*, 1999.

Kruse, F.A., "Spectral Identification of Image Endmembers Determined from AVIRIS Data," *Summaries of the Seventh JPL Airborne Earth Science Workshop*, 1998.

Kruse, F.A., Huntington, J.H. & Green, R.O., "Results from the 1995 AVIRIS Geology Group Shoot," *Proc. 2nd International Airborne Remote Sensing Conference and Exhibition*, 1996.

Lambert, P. & Chanussot, J., "Extending Mathematical Morphology to Color Image Processing," *CGIP'2000*, Saint-Etienne, France, 2000.

Landgrebe, D., "On Progress Toward Information Extraction Methods for Hyperspectral Data," *Proc. SPIE*, San Diego, CA, Aug.1997.

Otsu, N., "A Threshold Selection Method from Gray-Level Histograms," *IEEE Trans. Systems, Man, and Cybernetics*, Vol.SMC-9 No. 1, Jan. 1979.

Palmadesso, P., Antoniades, J., Baumback, M., Bowles, J. & Rickard, L.J., "Use of Filter Vectors and Fast Convex Set Methods in Hyperspectral Análisis," *Proceedings of SPIE*, 1999. Available at http://nemo.nrl.navy.mil/public/publications.html

Roberts, D.A., Dennison, P., Ustin, S., Reith, E., Morais, M., "Development of a Regionally Specific Library for the Santa Monica Mountains Using High Resolution AVIRIS Data," *Summaries of the Eighth JPL Airborne Earth Science Workshop*, 1999.

Sahoo, P.K., Soltani, S. & Wong, A.K.C., "A Survey of Thresholding Techniques," *Computer Vision, Graphics and Image Processing*, 41, pp. 233-260, 1988.

Serra, J., *Image Analysis and Mathematical Morphology*. Academic Press, London, 1982.

Serra, J., *Image Analysis and Mathematical Morphology, Volume 1*. Academic Press, London, 1993.

Soille, P., "Morphological Partitioning of Multispectral Images," *Journal of Electronic Imaging*, Vol. 5(3), pp. 252-265, July 1996.

Sternberg, S.R., "Greyscale Morphology," *Computer Vision Graphics and Image Processing*, 35, 283-305, 1986.

Szeredi, T., Staenz, K. & Neville, R., "Automated Endmembers Selection: Part I Theory," *Remote Sensing of Environment, 1999*.

Vane, G., Green, R.O., Chrien, T.G., Enmark, H.T., Hansen, E.G., Porter, W.M., "The Airborne Visible/Infrared Imaging Spectrometer (AVIRIS)," *Remote Sensing of Environment*, Vol. 44, pp. 127-143, 1993.

Winter, E.M. & Winter, M.E., "Autonomous Hyperspectral End-member Determination Methods," *Part of the EUROPTO Conference on Sensors, Systems and Next-Generation Satellites, Proc. SPIE*, Florence, Italy, Sep.1999.

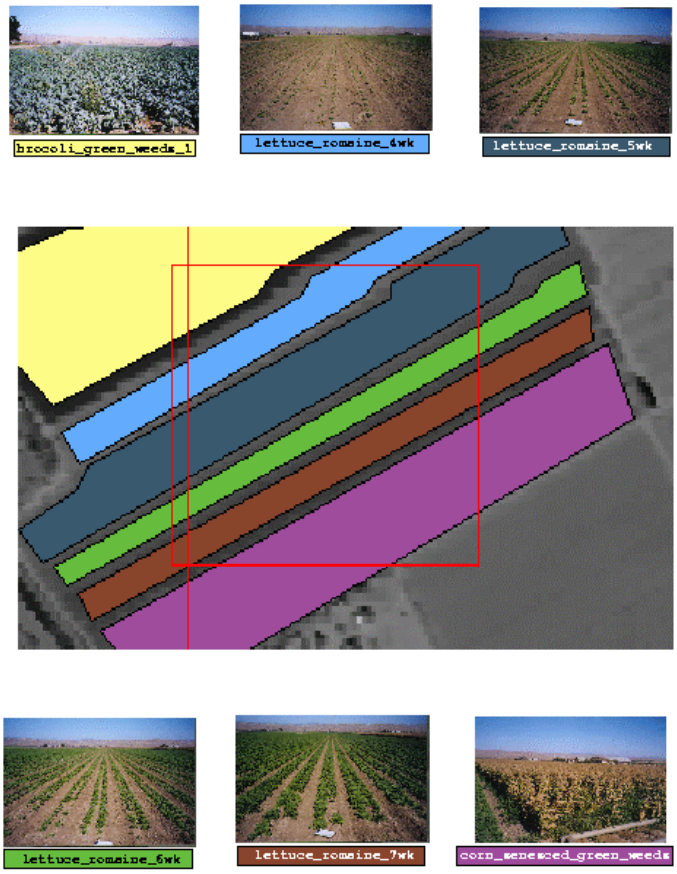

Figure 5. A subscene of the Salinas 98 dataset, showing known ground truth as polygons containing solid colors bounded by black lines and surrounded by thumbnail figures of the ground truth taken at the time of the data acquisition. The outlined box in red shows the subscene boundaries of the scene called Salinas A.

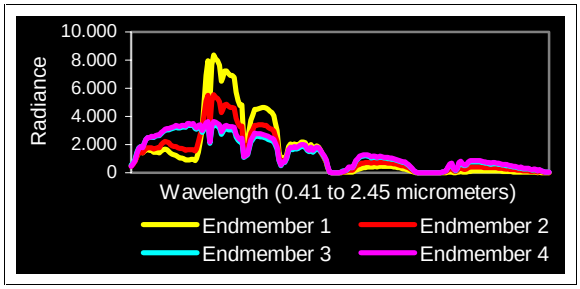

6.a)

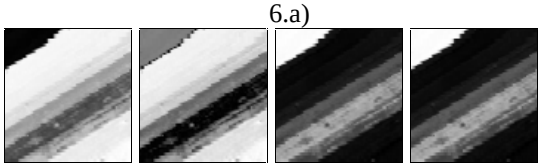

6.b) 6.c) 6.d) 6.e)

Figure 6. Resulting endmembers after applying AMEE method to the Salinas A dataset (a) and correspondent abundance maps (b-e).

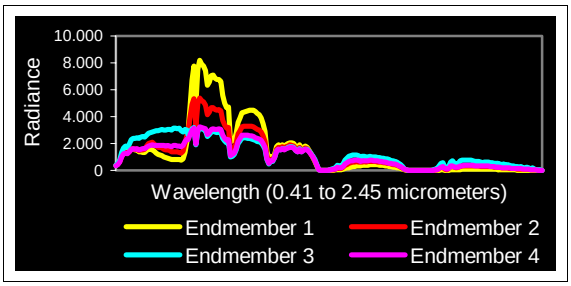

7.a)

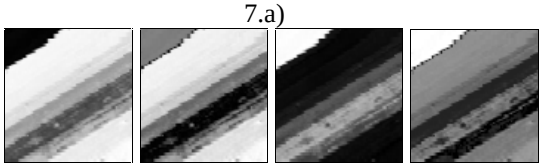

7.b) 7.c) 7.d) 7.e)

Figure 7. Resulting endmembers after applying PPI method to the Salinas A dataset (a) and correspondent abundance maps (b-e).